A Polarization Model Overcoming the Geometric Restrictions of the Laplace Solution for Spheroidal Cells: Obtaining New Equations for Field-Induced Forces and Transmembrane Potential

Jan Gimsa and Derk Wachner

Institut für Biologie, Humboldt-Universität zu Berlin, Berlin, Germany

ABSTRACT We present a new model for a variety of electric polarization effects on oblate and prolate homogeneous and single-shell spheroids. For homogeneous spheroids the model is identical to the Laplace model. For single-shell spheres of cell-like geometry the calculated difference of the induced dipole moments is in the thousandths range. To solve Laplace's equation for nonspherical single-shell objects it is necessary to assume a confocal shell, which results in different cell membrane properties in the pole and equator regions, respectively. Our alternative model addresses this drawback. It assumes that the disturbance of the external field due to polarization may project into the medium to a characteristic distance, the influential radius. This parameter is related to the axis ratio of the spheroid over the depolarizing factors and allows us to determine the geometry for a finite resistor-capacitor model. From this model the potential at the spheroid's surface is obtained and, consequently, the local field inside a homogeneous spheroid is determined. In the single-shell case, this is the effective local field of an equivalent homogeneous spheroid. Finally, integration over the volume yields the frequency-dependent induced dipole moment. The resistor-capacitor approach allowed us to find simple equations for the critical and characteristic frequencies, force plateaus and peak heights of deformation, dielectrophoresis and electrorotation for homogeneous and single-shell spheroids, and a more generalized equation for the induced transmembrane potential of spheroidal cells.

INTRODUCTION

The polarization of particles or biological cells can be investigated by measuring the impedance of suspensions (Asami et al., 1980; Foster and Schwan, 1996; Pauly and Schwan, 1959) or by a variety of single particle methods that exploit different force effects (Fuhr et al., 1985, 1996; Gascoyne et al., 1995; Georgieva et al., 1998; Gimsa et al., 1991; Hölzel, 1997; Maier, 1997; Pohl, 1978; Sukhorukov et al., 1998; Zimmermann and Arnold, 1983). Although impedance generally yields the same information as the single particle techniques e.g., dielectrophoresis (DP) and electrorotation (ER), the resolution of the latter methods for particle or cell properties is higher (Wang et al., 1993; Gimsa and Wachner, 1998). In the past, DP and ER required microscopic observation of the field-induced particle movement, a drawback that was recently overcome by automated video analysis (Gasperis et al., 1998; Hölzel, 1998; Schnelle et al., 1997) and by the introduction of light-scattering methods (Eppmann et al., 1999; Gimsa, 1999; Gimsa et al., 1997; Prüger et al., 1998). Besides characterization, polarization effects are increasingly applied not only for fusion and transfection of cells, but also for manipulation, trapping, or separation of biological particles and cells (Archer et al., 1993; Asbury and van den Engh, 1998; Becker et al., 1995; Fuhr et al., 1998; Gimsa, 1999; Hagedorn et al., 1992; Schnelle et al., 1996). In the future, applications to media and colloidal particles will be of growing interest (Arnold et al., 1987; Gimsa et al., 1998; Maier, 1997). For these practical applications a growing need for intuitive models and simplified equations describing the parameter dependences of polarization exists. The complexity of the present theory might be one of the reasons that the methods, regardless of their high potencies, have not yet found broader acceptance (see Kakutani et al., 1993; Pastushenko et al., 1988: Paul and Otwinowski, 1991; Sauer and Schlögl, 1985; Sokirko, 1992; Wang et al., 1993, 1997).

For biological cells the most striking frequency-dependent changes in polarizability result from structural (Maxwell-Wagner) polarization effects (Foster and Schwan, 1996; Gimsa and Wachner, 1998). Dielectric models consider the structural properties of cells by assuming spherical or ellipsoidal geometries in which a number of distinct media are arranged as core and shells (Fuhr et al., 1985; Gimsa et al., 1991, 1996; Kakutani et al., 1993; Müller et al., 1993; Pastushenko et al., 1985; Paul and Otwinowski, 1991; Sauer and Schlögl, 1985; Sokirko, 1992; Wang et al., 1997). When suspended in a low conductive medium, biological cells may exhibit two extreme cases of polarizability: they are either much less polarizable than the medium, or vice versa (Fig. 1). The first case applies for low frequencies, when the membrane effectively insulates the cell, the second for the medium frequency range, after capacitive membrane bridging, when the high cytoplasmic conductivity dominates polarization. At very high frequencies, where permittivity differences dominate polarization, cell polarizability is usually lower than that of the medium, mainly due to a disturbed water structure (Foster and Schwan, 1996). In

Received for publication 26 February 1999 and in final form 23 May 1999.

Address reprint requests to Jan Gimsa, Institut für Biologie, Humboldt-Universität zu Berlin, Invalidenstr. 42, D-10115 Berlin, Germany. Tel.: +49-30-2093-8494; Fax: +49-30-2093-8520; E-mail: Jan=Gimsa@rz.hu-berlin.de.

0006-3495/99/09/1316/11 $2.00

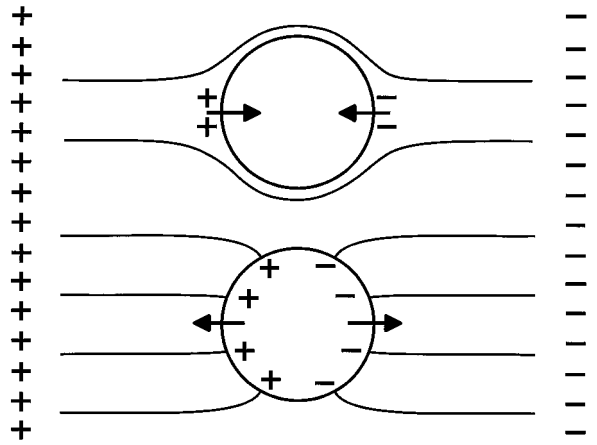

FIGURE 1 Field distribution for the two extreme cases of polarizability for a spheroidal object in a homogeneous field. Charge distributions are depicted for a DC- or for a certain moment of an AC-field. The resulting forces (*arrows*) may either tend to compress or elongate the object.

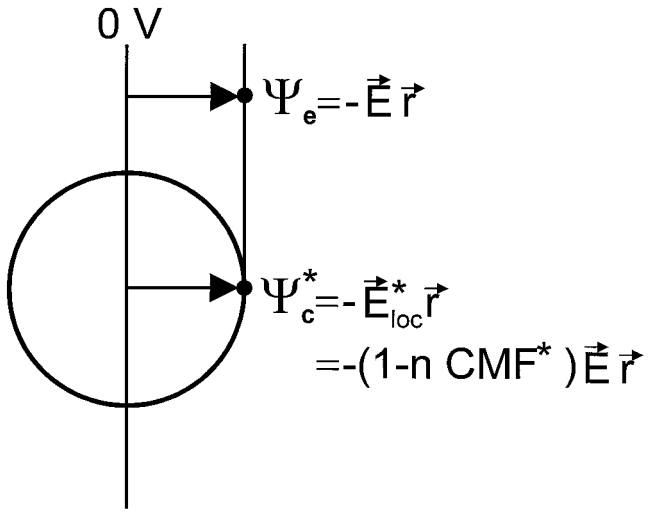

FIGURE 2 Induced potentials at the surface of a spheroid and in the external medium. The two points have equal distances to a symmetry plane perpendicular to the field direction. For simplicity, the potential at this plane can be assumed as 0 V. *CMF* and *n* stand for the Clausius-Mossotti factor, which is the frequency-dependent part of the induced dipole moment and the depolarizing factor, respectively (see below).

a homogeneous field cell deformation, elongation and compression can be observed (Krueger and Thom, 1997; Sukhorukov et al., 1998). In DP the inhomogeneous field results in unbalanced forces on the two hemispheres. As a result, particles or cells move toward or away from regions of high field depending on their polarizability relative to that of the suspension medium (Gimsa et al., 1991; Pastushenko et al., 1985; Pohl, 1978; Wang et al., 1993, 1997). The rotating ER field induces a rotating cell dipole moment. Any dispersion process causes a spatial phase shift of the external field vector and the induced dipole moment, giving rise to a permanent torque that may cause individual cell rotation in or against the rotation sense of the field (Gimsa et al., 1991; Pastushenko et al., 1985; Wang et al., 1993, 1997; Zimmermann and Arnold, 1983).

A simple notion of how the forces evolve is presented in Fig. 2. The difference of the potentials at the body's surface and the potential that would exist at the same site in the absence of the body ($\vec{E}\vec{r}$) causes forces that may be transformed into mechanical work, such as deformation, translation, or rotation. For a sphere with a depolarizing factor of $n = 1/3$ the Clausius-Mossotti factor (CMF) can take on values between 3 (extremely polarizable object, no local field) and -1.5 (nonpolarizable object, highest local field). For cells at low frequencies, the second case holds and most of the potential builds up over the membrane. Usually, in the literature one-third of the above CMF values is used (for explanation see below).

By the 1920s it had already been shown that, despite the complex geometry of the systems, suspensions of monodisperse homogeneous and single-shell particles exhibit only a single and double Lorentzian dispersion, respectively (for a historical introduction see Foster and Schwan, 1996). We were as surprised as these researchers when we recently found that a most simple resistor-capacitor (RC) model of cell polarization is equivalent to a spherical single-shell model (Gimsa and Wachner, 1998). The model allowed us to describe the two distinct dispersion processes observed in impedance, DP and ER, as well as the induced transmembrane potential. It assumes a cell suspension consists of elementary cubes, each of them containing a single cell and a certain volume of the surrounding medium. Internal and external media and the cell membrane were described by elements of prismatic geometry. This simplified geometry could easily be translated into an RC model. In the model, DP and ER are reflected by the real and imaginary part of the potential difference at the cell model's surface and a reference in the external medium, respectively. The impedance of the suspension was obtained by Kirchhoffs laws applied to a multitude of elementary cubes. We introduced the "influential radius," a parameter given by the characteristic length to which the field disturbance, induced by cell polarization, may potentially project into the suspension medium. The influential radius does not depend on frequency but only on cell shape. It determines the geometry of the RC model exhibiting the same frequency-dependence of induced potentials as the Laplace model. As mentioned in Gimsa and Wachner (1998) the RC model allows for an easy access to simplified solutions for the critical and characteristic frequencies, force plateaus and peak heights of deformation, DP, ER, and for the induced transmembrane potential. Only later we realized that the coincidence of these equations obtained for the influential radius of a sphere of 1.5 and the CMF of the Laplace solution was due to a coincidence of a volume factor of 3 and a depolarizing factor of spheres of $n = 1/3$ (compare Eqs. 1 and 8 below). To avoid further confusion in this paper we do not cancel the volume factor, which leads to a tripling of all CMF values but allows a clearer description for nonspherical objects. Some simple equations for spherical models like

Schwan's equation for the induced transmembrane potential or the time constant of membrane polarization already existed for a longer time (Foster and Schwan, 1996; Grosse and Schwan, 1992; Kinosita and Tsong, 1977; Pauly and Schwan, 1959; Zimmermann and Arnold, 1983). To our knowledge a complete set of simplified equations for the characteristic points of DP and ER spectra for a single-shell sphere was first derived by Gimsa et al. (1991) by row developments of the Laplace solution after introduction of area-specific parameters for the membrane.

In this paper we apply a new RC approach to the polarization of homogeneous and single-shelled, oblate, and prolate spheroids. For simplicity, we do not consider the impedance of suspensions and focus on a symmetry axis oriented perpendicular to the field. For calculation of the induced dipole moment we apply a notion of Maxwell to the spheroids, who stated that for spherically symmetric models for any field frequency an equivalent homogeneous sphere of the same radius can be found that experiences the same force or torque as the shelled model (Jones, 1995; Maxwell, 1873). Such a homogeneous equivalent spheroid must exhibit a constant internal (local) field, which leads to the induced dipole moment (Maxwell, 1873; Landau and Lifschitz, 1985). The local field can be calculated from the potential at one point of the spheroid's surface, e.g., the point given by a line parallel to the external field through the center of the spheroid. The potential at this point can easily be calculated from the new RC model, which assumes a prismatic volume element with an infinitely small cross-sectional area oriented along this line. The length of the element in the external solution for a given axis ratio and radius of the spheroid is given by the influential radius which depends on the electrostatic depolarizing factors. Finally, the induced dipole moment can be calculated from the local field (Landau and Lifschitz, 1985). For homogeneous spheroids our solution and the conventional Laplace solution are identical. For spherical single-shell objects of cell-like geometries the difference of the two solutions is in the thousandths range and related to the impedance properties of membrane, core, and exterior. For oblate and prolate spheroids the new model overcomes the assumption of a confocal layer or membrane of ill-defined thickness, which is necessary to solve Laplace's equation. Comparison of DP and ER spectra obtained from the Laplace and RC models revealed that the antifield ER peak is influenced by the equatorial membrane properties as well as by the axis ratio of the spheroid. When the volume of a single-shell spheroid was changed by changing the axis ratio at a constant radius in the Laplace model, opposite frequency shifts of the antifield peak were found for constant membrane properties at equator and poles. The behavior of our model is close to the Laplace case with constant equatorial membrane properties.

The RC approach allowed us to specifically simplify the electric scheme for consideration of critical and characteristic frequencies, force plateaus, and peak heights of DP and ER as well as for the transmembrane potential. The characteristic equations derived contain the axis ratio as a free parameter and include the solutions known for homogeneous and single-shell spheres. Thus, our model offers easy access to an understanding of basic parameter dependencies of cell polarization and can be used for a qualitative interpretation of data or fast, nonlinear data fitting. The concept also offers a simple approach to the phenomena of impedance, orientation, electrooptics, and pearl chain formation, which are not considered in this paper. Also, there is hope that it can principally be applied to derive approximate analytical equations for objects of nonellipsoidal shape. For a more general introduction please see Gimsa and Wachner (1998).

THE MODEL

The induced dipole moment of spheroids

The dipole moment of a homogeneous spheroid with the axes r, r, and c is given by the volume integral of the polarization $\vec{P}$, which is constant over the volume. Thus, for media of low loss the dipole moment can be written as:

$$\vec{m}^* = \frac{4\pi r^2 c}{3}\vec{P}^* = \frac{4\pi r^2 c}{3}\epsilon_e\epsilon_0\vec{E}\mathrm{CMF}^* \qquad (1)$$

where $\vec{E}$, CMF*, and $\epsilon_e\epsilon_0$ stand for the external field, the frequency-dependent CMF, and the permittivity of the external medium. The asterisk denotes complex variables. In the following, when no arrows designate vectors in equations the absolute value of the vector is used. The external field has no imaginary component. CMF* in Eq. 1 is the complex form of the solution for homogeneous ellipsoids given by Landau and Lifschitz (1985):

$$\mathrm{CMF}^* = \frac{\epsilon_i^* - \epsilon_e^*}{\epsilon_e^* + (\epsilon_i^* - \epsilon_e^*)n} = 3\ \mathrm{CMF}^*_{\mathrm{classic}} \qquad (2)$$

where ϵ_i^*, ϵ_e^* and n stand for relative internal and external permittivities and the depolarizing factor. The CMF defined by Eq. 2 differs from the $\mathrm{CMF}^*_{\mathrm{classic}}$ used by most authors by a factor of 3. The advantage of Eq. 2 is that for the dipole moment (Eq. 1) the complete volume term is conserved.

According to Landau and Lifschitz (1985) the local field within a homogeneous ellipsoid is given by:

$$\vec{E}^*_{\mathrm{loc}} = \vec{E} - \frac{n\vec{P}^*}{\epsilon\epsilon_0} \qquad (3)$$

For the symmetry axis of the spheroid being perpendicular to the external field polarization, the external and local field will be in parallel, and the fields in Eq. 3 can be expressed by potentials according to Fig. 2:

$$\vec{P}^* = \frac{\epsilon_e\epsilon_0}{n}(\vec{E} - \vec{E}^*_{\mathrm{loc}}) = \frac{\epsilon_e\epsilon_0}{n}\left(\frac{\psi_e - \psi_c^*}{\psi_e}\right)\vec{E} \qquad (4)$$

where ψ_c^* is the potential at the surface of the spheroid that can be obtained from the RC model (see below).

Geometry of the model

In a previous paper we assumed a prismatic cell geometry limited by two parallel membrane planes of arbitrary shape (Gimsa and Wachner, 1998). Polarization, and consequently the forces experienced by the cell, were described by the difference of the potential at the surface of the model and

a reference potential (compare Fig. 2 and Eq. 4). The reference potential was frequency-independent and could be obtained in the external solution at radius distance from the symmetry plane. A more suggestive notion is that the reference is given by the potential that would exist at the site of the model surface in the absence of the cell. In this paper we do assume a prismatic volume element with an infinitely small cross-sectional area of arbitrary but constant shape. The element is oriented in field direction along a line through the center and equator of the cell (Fig. 3). Please note that for an orientation of the symmetry axis of the spheroid parallel to the field, the element will be oriented along this axis.

In Fig. 4 the impedance Z_j^* in field direction for the medium with index j is given by cross-sectional area A_j and length d_j;

$$Z_j^* = \frac{1}{\sigma_j^*}\frac{d_j}{A_j} \tag{5}$$

where σ_j^* is the complex conductivity:

$$\sigma_j^* = \sigma_j + j\omega\epsilon_j\epsilon_0 \tag{6}$$

which is described by its frequency-independent DC conductivity σ_j and its relative permittivity ϵ_j. j, ω, and ϵ_0 stand for $(-1)^{0.5}$, circular frequency, and permittivity of vacuum, respectively. It can easily be shown that Eq. 5 is equivalent to a parallel resistor-capacitor (RC) pair of the same geometry (Foster and Schwan, 1996; Gimsa and Wachner, 1998).

Electric model

The potential at the cell surface, ψ_c^*, depends on field frequency, electrical, and geometrical properties:

$$\psi_c^* = \frac{Z_i^* + Z_m^*}{Z_i^* + Z_m^* + Z_e^*}\vec{E}r_{infl} \tag{7}$$

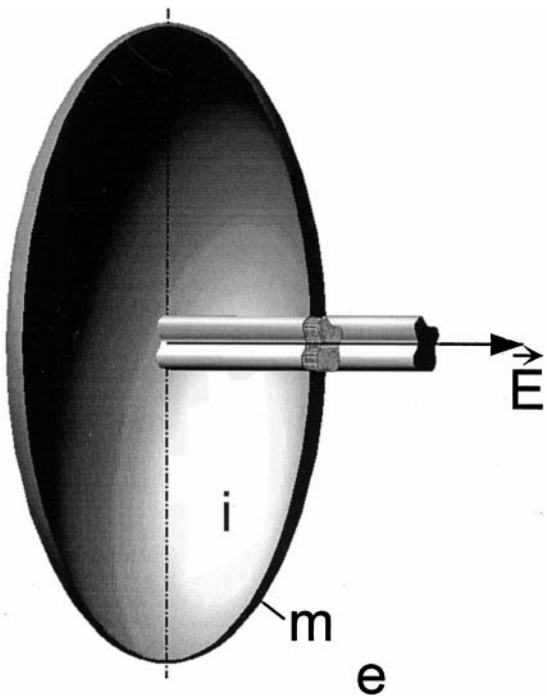

FIGURE 3 Spheroidal, single-shell cell model with a confocal membrane of nonconstant thickness. *i*, *m*, and *e* designate cytoplasm, membrane, and external medium, respectively. The field is applied perpendicular to the symmetry axis. The RC model considers a prismatic volume element with an infinitely small cross-section.

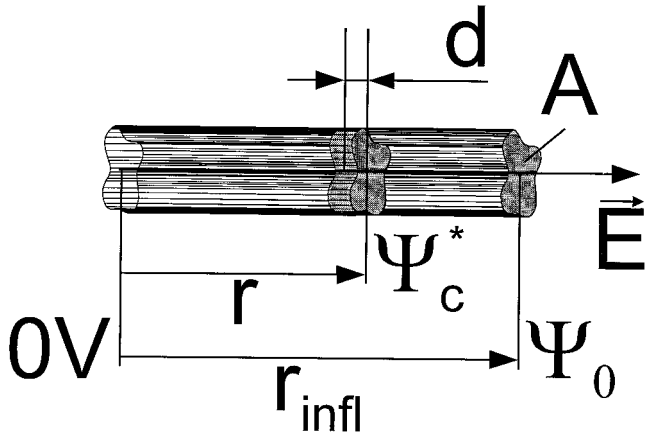

FIGURE 4 Sketch of the prismatic volume element of Fig. 3. A, d, r, and r_{infl} stand for cross-sectional area, membrane thickness, equatorial radius of the spheroid (cell radius), and influential radius. $\vec{E}$, ψ_c^*, and ψ_0 are the external field strength, and the potentials at the cell surface as well as at the influential radius (the maximum potential at the cell surface). For symmetry reasons the induced potential in the center of the cell can be assumed to be 0 V.

with Z^* being the impedances of the prismatic elements of Fig. 4 (compare to Fig. 5). From Eq. 7 it is obvious that the maximum induced potential for a cell insulated by a nonconducting membrane at DC or low frequencies is determined by r_{infl}. In this case ψ_c^* directly reflects the geometry of the model and may be amplified in comparison to ψ_e, e.g., by 1.5 for a nonconducting spherical object with $r_{infl} = 1.5r$ (Gimsa and Wachner, 1998). Equation 7 can be further simplified by eliminating the cross-sectional areas (see Eq. 5), which are equal for the three prismatic elements. The membrane thickness, d, can be eliminated by introduction of area-specific conductivity and capacitance, as well.

The Clausius-Mossotti factor (CMF)

Following a notion of Maxwell (1873), for any field frequency an equivalent homogeneous spheroid of the same geometry can be found which experiences the same force or torque as the shelled object. Equations 3, 4, and 7 can be used to calculate the local field for this Maxwellian homogeneous equivalent spheroid. Within this equivalent spheroid the polarization is assumed to be constant over the volume. Thus, the induced dipole moment is given by the product of polarization and volume (Eq. 1). Finally, comparison of Eqs. 1 and 4 yields the complex CMF in the form:

$$\mathrm{CMF}^* = \frac{1}{n}\left(\frac{\psi_e - \psi_c^*}{\psi_e}\right) \quad \text{with} \quad \psi_e = \frac{r}{r_{infl}}\psi_0 \tag{8}$$

The CMF is the frequency-dependent part of the induced dipole moment which is, according to the common dipole approximation models, proportional to the frequency-dependence of ponderomotive force effects like deformation, DP translation, or ER rotation. To calculate these effects the respective mechanism of interaction of the induced dipole moment with the external field has to be taken into account (Fuhr et al., 1985; Gimsa et al., 1991; Pastushenko et al., 1985; Sauer and Schlögl, 1985; Wang et al., 1997).

Dependence of axis ratio and influential radius on depolarizing factors

Equations 1 and 2 contain the depolarizing factor of the ellipsoid (Landau and Lifschitz, 1985). Explicit expressions for the depolarizing factors of spheroids were first derived by Stille (1944). For our model the depolar-

izing factor n in field direction for oblate (Eq. 9A) and prolate (Eq. 9B) spheroids is given by:

$$n = \frac{1}{2}\left[1 - \frac{1+e^2}{e^3}(e - \arctan e)\right] \quad \text{with} \quad e = \sqrt{\left(\frac{r}{c}\right)^2 - 1} \tag{9A}$$

and

$$n = \frac{1}{2}\left[1 - \frac{1-e^2}{2e^3}\left(\ln\frac{1+e}{1-e} - 2e\right)\right] \quad \text{with} \quad e = \sqrt{1 - \left(\frac{r}{c}\right)^2} \tag{9B}$$

respectively, where e stands for the excentricity. Spheroids possess two equal axes with the third, in our case, lying perpendicular to the field. The sum of the three depolarizing factors for the three axes of an ellipsoid must always be unity. Thus, if the depolarizing factor in the direction of the third axis is 1, the one in field direction must vanish (infinitely thin disk), whereas it will be 0.5 in field direction if the depolarizing factor in the direction of the third axis vanishes (infinitely long cylinder; see Fig. 6)

For a given axis ratio (depolarizing factor) the CMF of a spheroid may theoretically reach two extreme values, which correspond to the two extreme cases for the relative polarizabilities of medium and object. Biological cells, insulated by their low conductive membrane of high specific capacitance may, depending on field frequency, approach these two cases when suspended in a low conductive medium (Fig. 7).

The equations for the minimum and maximum of the CMF given in Fig. 7 are obtained from Eq. 2. They must correspond to the extrema of the local field and the potential ψ_e^*, respectively. The CMF maximum corresponds to a local field of 0 V/m, whereas the CMF minimum is reached for the highest local field. The local field strength may exceed the external field to a degree that depends on the shape of the object, e.g., by a factor of 1.5 for spheres (this can easily be tested for $n = 1/3$ with the equations given in Fig. 2). In Eq. 3 the shape dependence of the local field is expressed by the depolarizing factor n. In the RC model (Fig. 5) the local field is given by ψ_c^*/r. Its maximum corresponding to the minimum in CMF is ψ_0/r. This leads to the relation of r_{infl} and n:

$$\frac{r_{infl}}{r} = \frac{1}{1-n} \qquad \xi = \frac{r_{infl}}{r} - 1 \tag{10}$$

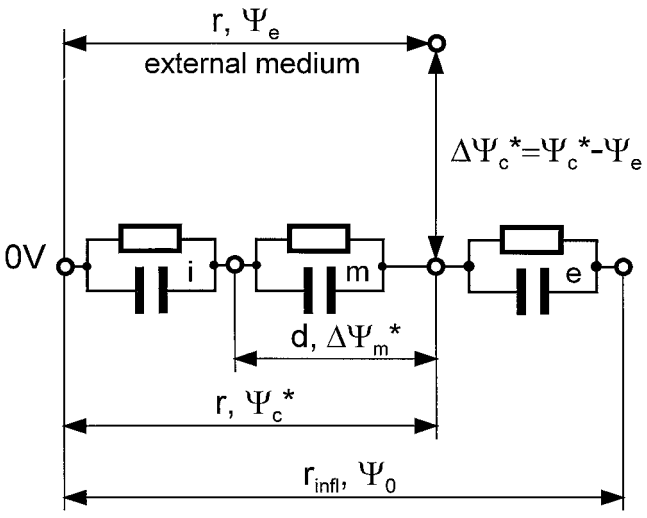

FIGURE 5 RC model for Fig. 4. The RC pairs *i*, *m*, *e* describe the properties of the three media. ψ_e is the reference potential in the external solution at distance r from the symmetry plane, which is given by $(r/r_{infl})\psi_0$ (see Fig. 2). Over membrane thickness d the potential difference $\Delta\psi_m^*$ is induced.

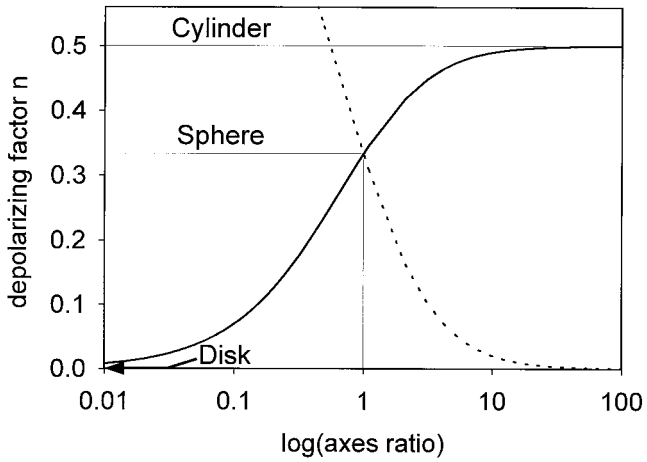

FIGURE 6 Depolarizing factor of the spheroid in the equatorial plane (*solid line*) and along the symmetry axis (*dotted line*) as a function of axis ratio.

which allows us to establish the dependence of r_{infl} on the axis ratio of the spheroid (Fig. 8). Here we also define ξ, which will be used to simplify the expressions of the characteristic equations below. Now, starting from Eqs. 7 and 8 the CMF can be expressed by the impedances of the prismatic elements (Figs. 4 and 5).

$$\begin{aligned} \mathrm{CMF}^* &= \frac{1}{n}\left(1 - \frac{Z_i^* + Z_m^*}{Z_i^* + Z_m^* + Z_e^*}\frac{r_{infl}}{r}\right) \\ &= \frac{1+\xi}{\xi}\left(1 - \frac{Z_i^* + Z_m^*}{Z_i^* + Z_m^* + Z_e^*}(1+\xi)\right), \end{aligned} \tag{11}$$

for a spherical cell $n = 1/3$ and $r_{infl} = 1.5r$. Its CMF value depends on the impedances of the elements. At low frequencies for the case of no membrane conductivity Z_m^* exceeds the other impedances, yielding a CMF value of -1.5. In the medium frequency range for a cytoplasmatic conductivity infinitely higher than the external conductivity and complete membrane bridging CMF may approach the other extreme value of 3 for $(Z_i^* + Z_m^*)$ approaching 0.

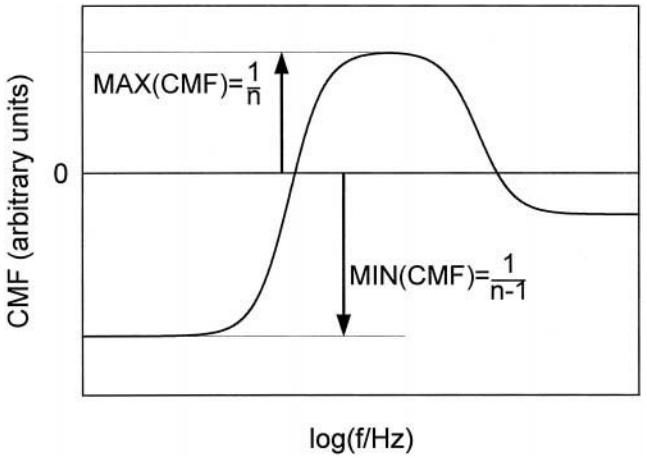

FIGURE 7 Schematic drawing of the frequency dependence of the CMF of a cell-like object, with low and high relative polarizability at low and medium frequencies, respectively. At very high frequencies the polarizability is determined by the ratio of core and medium permittivities.

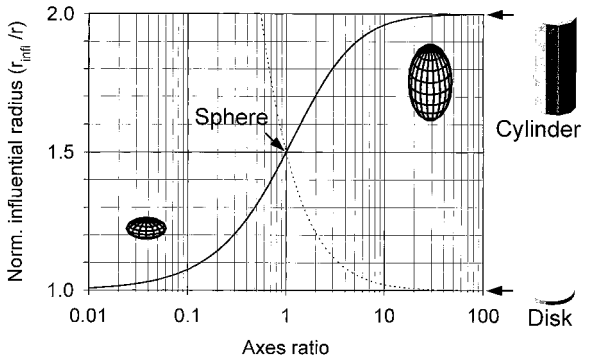

FIGURE 8 Normalized influential radii of spheroids as a function of the axis ratio. The normalized influential radius in the equatorial plane (*solid line*) approaches 1 and 2 for an infinitely thin disk and an infinitely long cylinder, respectively. The dotted line represents the normalized influential radius in the direction of the symmetry axis. The normalized influential radii reflect the maximum local field amplification.

DISCUSSION

Comparison of Laplace and RC models

As a consequence of the mechanisms of DP and ER their frequency spectra reflect real and imaginary (out of phase) parts of the induced dipole moment (Fuhr et al., 1985; Gimsa et al., 1991; Pastushenko et al., 1985; Wang et al., 1997). Since field strength (in DP and ER) and field gradient (in DP) as well as friction coefficients are not very well defined, for theoretical considerations usually the CMF is used to describe the frequency-dependence of the induced dipole moment. To test our model, we analytically and numerically compared the CMF of Laplace and RC models using the software Mathematica and Maple. For homogeneous spheroids the expressions for the induced dipole moment of the Laplace and our new model were found to be identical. For single-shell spheroids of different axis ratios we numerically checked that the homogeneous spheroid is the limiting case for both models, Laplace and RC, for vanishing shell thickness as well as for a shell thickness equal to the cell radius. For spherical single-shell models the difference of the two models depends on shell thickness as well as on the electrical properties of core, shell, and external medium. These interrelations were discussed by Pastushenko et al. (1988) for spherical multishell models. For cell-like parameters (see Table 1) the difference is in the thousandths range; an example is given in Fig. 9. These considerations suggest that the model can be applied nicely to spherical cells but not evenly well to smaller objects with relatively thick shells like viruses (see Gimsa, 1999) or to objects with highly conductive shells. Fortunately, because of the shielding effect it can be assumed that for the latter case the geometric restrictions of Laplace modeling will cause only small errors.

The next step was to compare the Laplace and RC spectra of single-shell spheroids with different axis ratios. In the following the theoretical model behavior is considered in terms of DP and ER spectra, since they separately reflect the real and imaginary parts of the CMF, respectively. For calculations we kept the equatorial radius constant and changed the axis ratio in the range from 1:10 (oblate) to 10:1 (prolate). As expected, the high frequency DP plateau and the ER cofield (internal bulk) peak exhibited the same axis ratio-dependence (Fig. 10). In all cases this peak was identical to the behavior of a homogeneous model with the properties of the core. To test the influence of the membrane shell, for the Laplace model two different cases with constant membrane area-specific properties at the equator and at the poles, respectively, were considered (Fig. 10, *A* and *B*). This was achieved in two different ways. In one case the parameters were kept constant by keeping the membrane thickness constantly at 8 nm at the equator (Fig. 10 *A*) and the poles (Fig. 10 *B*), respectively. The other way was to compare the case of Fig. 10 *A* to the case of constant area-specific membrane properties at the poles, which was achieved by adjusting membrane capacitance and conductance (not shown). No significant differences were found for the different ways of keeping the membrane properties constant.

TABLE 1 Standard parameters for model calculations on the single-shell spheroid

Parameter	Value
Axis length along the symmetry axis (*c*)	0.5 μm–50 μm
Equatorial radius (*r*)	5 μm
Membrane thickness (*d*)	8 nm
Conductivity	
Internal	0.53 S/m
Membrane	10^{-6} S/m
External	0.12 S/m
Relative permittivity	
Internal	50
Membrane	9.04
External	80

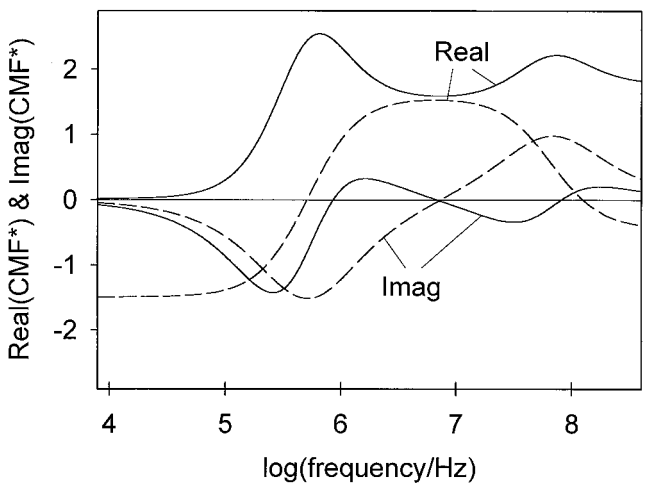

FIGURE 9 Theoretical DP (Real(CMF*)) and ER (Imag(CMF*)) spectra of a spherical single shell model with the parameters given in Table 1 (*dashed lines*). The differences of the Laplace and RC models become visible only by multiplication by 1000 (*solid lines*).

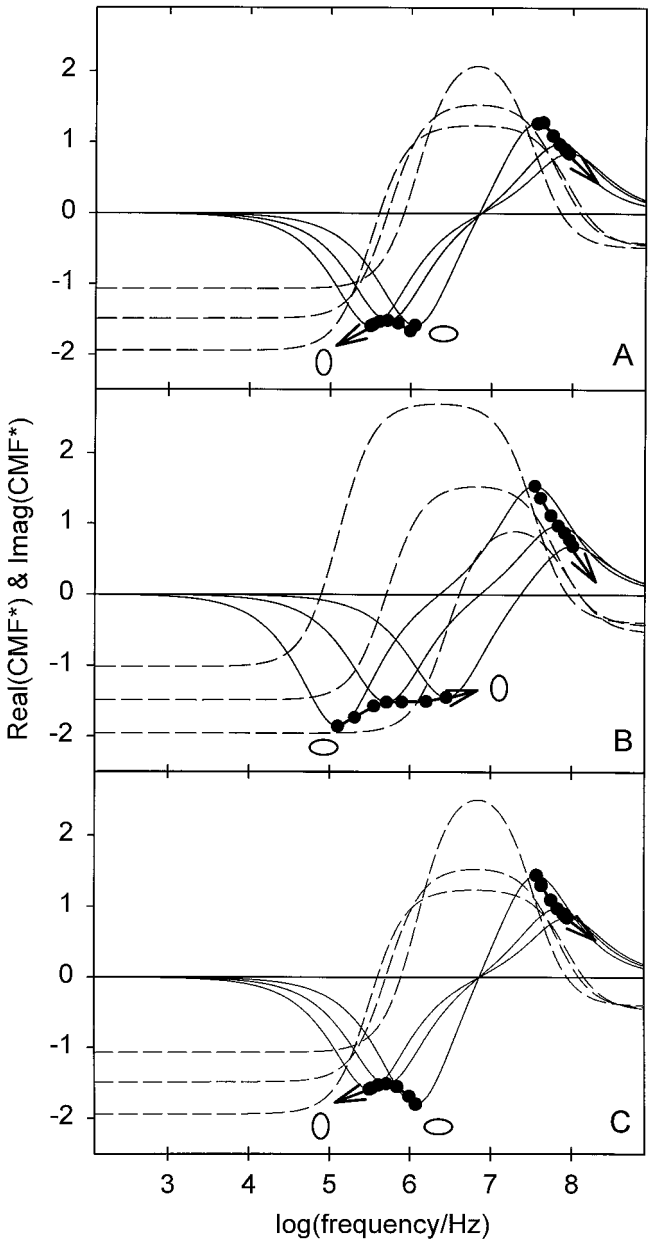

FIGURE 10 Real (*dashed lines*) and imaginary (*solid lines*) parts of the CMF over frequency for a cell-like model calculated by Laplace (*A* and *B*) and RC models (*C*) for 1:10 (oblate), 1:1 (sphere), and 10:1 (prolate) spheroids. Model parameters are given in Table 1. The radius was kept constant. To change the axis ratio the length of axis *c* was changed (increase marked by *arrow*). In *A* and *B* the membrane thickness was constant at the equator and the poles, respectively. The peaks of the imaginary part of CMF are marked for axis ratios of 1:10, 1:5, 1:2, 1:1, 2:1, 5:1, and 10:1.

For the antifield ER peak behavior striking differences were found in between the two Laplace cases (Fig. 10, *A* and *B*). For a volume of the spheroid increasing with an increasing *c* axis, the characteristic frequency of the antifield peak (first characteristic frequency; f_{c1}) of the membrane reduces (Fig. 10 *A*). This is consistent with a spherical single-shell model for which it is theoretically and experimentally proven that a volume increase at a constant membrane thickness leads to a decrease of f_{c1}, due to the overall increase in membrane capacitance. The f_{c1} behavior in Fig. 10 *B* is in sharp contrast to this behavior. To understand these properties of the Laplace model one has to keep in mind the physical reason for the geometrical restrictions to the models. The prerequisite for an explicit solution of Laplace's equation is that the objects have surfaces of the second degree. The ellipsoid is the most complex surface of the second degree that is finite. The ellipsoidal shape allows for a constant field in the core, ensuring that the second derivative of the (induced) potential function is 0 and still defined at zero-radius. In the single-shell case for an explicit solution all interfaces need to be described within the same coordinate system, which is determined by the foci of the ellipsoid. For spheroids of a given radius, as in our case, the foci determine the axis ratio and in turn the deviation in equatorial and polar membrane thickness, i.e., properties. The other side of the coin obviously is that confocal shells with nonconstant thickness (Fig. 3) allow for a constant core field, which was the prerequisite for an analytical Laplace solution. This suggests that in the prolate case the lower shielding at the poles due to the decrease in membrane thickness is essential for the constant core field. These considerations suggest that no constant field can be assumed in the cytoplasm of ellipsoidal cells with a constant membrane thickness.

The membrane polarization dependence on the axis ratio presented in Fig. 10 *A* agrees with the RC model. The latter model calculates the induced dipole moment at a given frequency for an equivalent homogeneous spheroid. The model assumes a constant field for the whole volume of the equivalent spheroid. Thus, in both RC and Laplace models, the boundary conditions for the field ensure that Maxwellian-equivalent spheroids with constant fields exist, which are nonetheless different. By demanding constant fields for both the core and the equivalent body, the Laplace model is much stiffer than the RC model.

Characteristic equations derived by simplified schemes

As already discussed in Gimsa and Wachner (1998) the RC approach allows the easiest simplifications for the derivation of equations which describe the main parameter dependences of characteristic points of cell deformation, DP, ER, induced transmembrane potential, etc. While the deformational and DP forces are proportional to the real part of the CMF, the ER torque is proportional to its imaginary part. The CMF is related to $\Delta\psi_c^*$ (Fig. 5, Eq. 8) and depends on the axis ratio and influential radius as described by Eq. 11. Except for rotating fields, the following considerations are also valid for a symmetry axis pointing in field direction when the corresponding influential radius is taken into account.

The scheme of Fig. 5 can be simplified in different ways to describe the three polarization plateaus and two disper-

sion processes leading from one to the other (Fig. 11). All simplified schemes are given in Fig. 12. With increasing frequency, starting at DC the plateaus can be described by schemes A, B, and C:

Scheme A, first plateau: For DC and frequencies still too low for capacitive membrane bridging the ionic conductivities of all media determine the polarization. The Ohmic resistance of the cell membrane represents the highest impedance. The external membrane side of the cell will be charged to a potential close to ψ_0. In analogy the internal membrane side is close to a potential of 0 V. Accordingly, the induced transmembrane potential $\Delta\psi_m$ is at maximum.

Scheme B, second plateau: After capacitive membrane bridging the polarization is described by the balance of the ionic conductivities of internal and external medium. The induced transmembrane potential vanishes.

Scheme C, third plateau: Frequency-independent ionic conductivities are superseded by capacitive currents and the polarization is described by the permittivity balance of internal and external medium.

Schemes D and E describe the transitions in between the plateaus A and B (β1 dispersion) and B and C (β2 dispersion). Each dispersion yields a phase shift between external field and cell surface potential, generating an ER torque in a rotating field. The torque is proportional to the imaginary part of the CMF (for discussion see Gimsa and Wachner, 1998). Scheme D also describes the frequency-dependence of the dispersing transmembrane potential.

To derive characteristic equations the membrane properties were expressed by area-specific conductance ($g = \sigma_m/d$) and capacitance ($C = \epsilon_0\epsilon_m/d$) (compare to Eq. 5). For DP spectra and cell deformation the following characteristic equations were found:

$$F_1 = (\xi + 1)\frac{rg(\sigma_i - \sigma_e) - \sigma_i\sigma_e}{rg(\xi\sigma_i + \sigma_e) + \sigma_i\sigma_e}$$

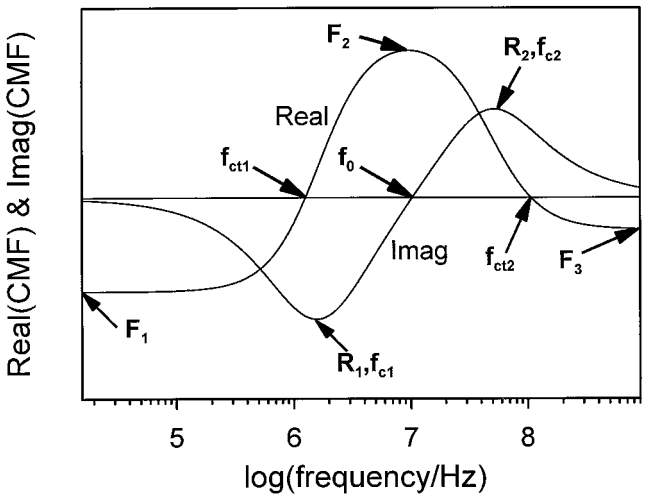

FIGURE 11 Schematic DP (Real(CMF*)) and ER (Imag(CMF*)) spectra. For DP, characteristic force plateaus (F_1, F_2, F_3) and critical frequencies (f_{ct1}, f_{ct2}), for ER torque peaks (R_1, R_2), characteristic frequencies (f_{c1}, f_{c2}) and the characteristic frequency of no torque (f_0) are marked.

$$F_2 = \frac{(\xi + 1)(\sigma_i - \sigma_e)}{\xi\sigma_i + \sigma_e}$$

$$F_3 = \frac{(\xi + 1)(\epsilon_i - \epsilon_e)}{\xi\epsilon_i + \epsilon_e}$$

$$f_{ct1} = \frac{1}{2\pi rC}\sqrt{\frac{\sigma_e^2\sigma_i^2 - \sigma_e\sigma_i rg((1 - \xi)\sigma_i - 2\sigma_e)}{(\sigma_i - \sigma_e)(\sigma_e + \xi\sigma_i)} - r^2g^2}$$

$$f_{ct2} = \frac{1}{2\pi\epsilon_0}\sqrt{\frac{(\sigma_i - \sigma_e)(\sigma_e + \xi\sigma_i)}{(\epsilon_e - \epsilon_i)(\epsilon_e + \xi\epsilon_i)}} \tag{13}$$

The characteristic equations for ER spectra are:

$$R_1 = \frac{-(\xi + 1)^2\sigma_i^2\sigma_e}{2(\sigma_e + \xi\sigma_i)(rg(\sigma_e + \xi\sigma_i) + \sigma_e\sigma_i)}$$

$$R_2 = \frac{(\xi + 1)^2(\sigma_i\epsilon_e - \epsilon_i\sigma_e)}{2(\sigma_e + \xi\sigma_i)(\epsilon_e + \xi\epsilon_i)}$$

$$f_{c1} = \frac{1}{2\pi rC}\left(\frac{\sigma_e\sigma_i}{\sigma_e + \xi\sigma_i} + rg\right)$$

$$f_{c2} = \frac{1}{2\pi\epsilon_0}\frac{\sigma_e + \xi\sigma_i}{\epsilon_e + \xi\epsilon_i}$$

$$f_0 = \frac{1}{2\pi}\sqrt{-\frac{\epsilon_0 rg^2(\epsilon_e\sigma_i - \epsilon_i\sigma_e) + \sigma_i^2(\epsilon_0\epsilon_e g - C\sigma_e)}{\epsilon_0 rC^2(\epsilon_e\sigma_i - \epsilon_i\sigma_e) + \epsilon_0^2\epsilon_i^2(\epsilon_0\epsilon_e g - C\sigma_e)}} \tag{14}$$

where f_0 is the frequency between the two ER peaks where no torque is induced and Imag(CMF*) = 0 (Fig. 11). Although this equation was obtained from the complete RC model it surprisingly does not depend on ξ (compare to Fig. 10, *A* and *C*). For cell parameter determination this is a very interesting feature. Moreover, f_0 can be measured by "natural compensation" since the external rotating field frequency needs only be changed to the frequency where rotation ceases. Thus, in the future f_0 might be especially interesting for ER light scattering (Gimsa, 1999; Prüger et al., 1997, 1998).

For a spherical model ($\xi = 0.5$) all equations except those for R_2 and f_0 reduce to the expressions already given by Gimsa et al. (1991; appendix A). The difference in the old R_2 expression was obviously caused by the more complex way of derivation; f_0 now contains the membrane conductivity. Under certain conditions all equations can be further simplified. Especially interesting for biological cells is the case of no membrane conductivity, leading to:

$$f_{ct1} = \frac{1}{2\pi rC}\sqrt{\frac{\sigma_e^2\sigma_i^2}{(\sigma_i - \sigma_e)(\sigma_e + \xi\sigma_i)}}$$

$$f_{c1} = \frac{1}{2\pi rC}\left(\frac{\sigma_e\sigma_i}{\sigma_e + \xi\sigma_i}\right)$$

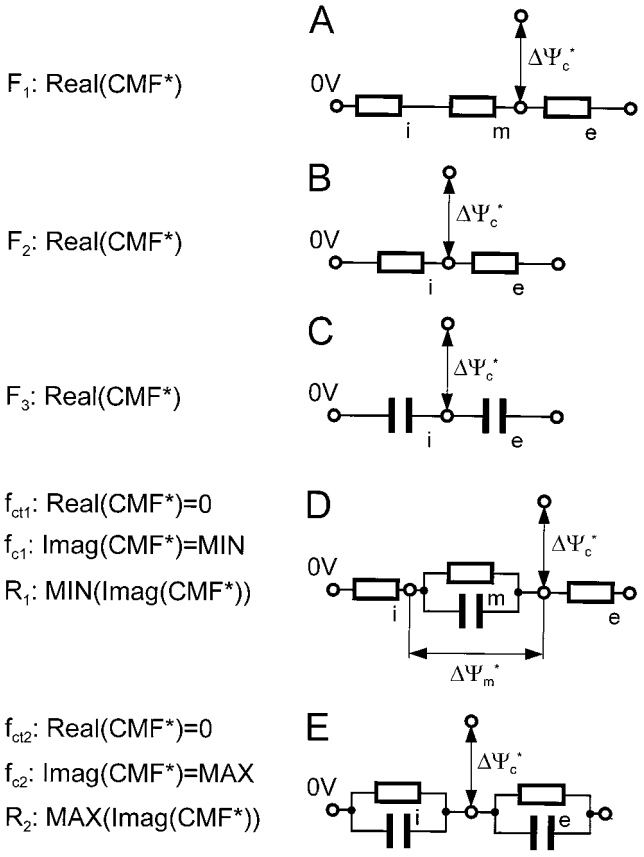

FIGURE 12 Criteria and simplified schemes for the derivation of the DP and ER spectra characteristics according to Fig. 11.

$$f_0 = \frac{\sigma_i}{2\pi}\sqrt{\frac{1}{rC\epsilon_0\left(\epsilon_e\frac{\sigma_i}{\sigma_e} - \epsilon_i\right) - \epsilon_0^2\epsilon_i^2}} \tag{15}$$

Please note that for cells the term $\epsilon_0\epsilon_i$ in the f_0 equation has a very small value and can usually also be omitted. If it is further assumed that $\xi\sigma_i \gg \sigma_e$, a condition that corresponds to the case of $\sigma_i \gg \sigma_e$ for a single shell sphere, one obtains:

$$f_{ct1} = \frac{\sigma_e}{\sqrt{\xi}2\pi rC} \qquad f_{c1} = \frac{\sigma_e}{\xi 2\pi rC} \tag{16}$$

For the induced transmembrane potential an axis ratio-dependent expression was obtained. Assuming complete membrane bridging at high frequencies, the absolute peak value is given by:

$$|\Delta\psi_m^*| = \frac{(1+\xi)rE}{\left(1 + rg\left(\frac{1}{\sigma_i} + \frac{\xi}{\sigma_e}\right)\right)\sqrt{1 + \frac{f^2}{f_{c1}^2}}} \tag{17}$$

where E, f, and f_{c1} stand for the peak value of the external field strength, the frequency of the external field, and the characteristic frequency of the membrane charging process as given by Eq. 14, respectively. It is clear that the spheroidal shape needs to be considered when the angle-dependence of the induced transmembrane potential is described. For $\xi = 0.5$ Eq. 17 reduces to the well-known Schwan equation (Foster and Schwan, 1996; Grosse and Schwan, 1992).

CONCLUSIONS

The goal of this paper was to first present a new dipole approach to modeling particle and cell polarization, and second to derive characteristic equations for deformation, DP, ER, and the induced transmembrane potential. To keep this first model presentation simple we focused on homogeneous and single-shell spheroids with the symmetry axis oriented perpendicular to the field. This symmetry and orientation ensured that for a rotating field the depolarizing factor and influential radius are constant during one cycle of the field and their values are the same for DP and ER fields. The model can be considered as a special finite element description along a line through the equator and center of the spheroid. The prerequisite for this approach with finite elements possessing a tremendous dimension difference in diameter and length is the parallel orientation of internal and external field within the considered elements. This assumption of a parallel orientation generally also holds for ER when the spatial angle between internal and external fields is considered a transformed phase angle. Nevertheless, a similar RC approach may also help overcome the generally applied simplification of DP fields with negligible inhomogeneity. Also, the extension to randomly oriented single-shell general ellipsoids is possible (manuscript in preparation). A more complicated problem might be the extension to multishelled ellipsoids or nonellipsoidal objects. Such detailed investigations of the model are still underway and a possible problem will be that the Laplace solution can no longer serve as a reference. Also, conventional finite element descriptions of cells are problematic since they will suffer from the huge difference in the dimensions of core and membrane shell.

We believe that the Laplace description of biological cells or evenly coated objects by the common confocal spheroidal models may lead to large errors in the case of extreme axis ratios. These errors, arising from an ill-defined layer thickness, will also be found for the general ellipsoidal case. For a thin, low conductive membrane layer our description seems to be superior over the Laplace approach. We also assume that the Laplace description of biological cells with internal membrane systems by confocal multi-shell ellipsoids is problematic (Jones, 1995; Kakutani et al., 1993; Müller et al., 1993; Paul and Otwinowski, 1991; Sokirko, 1992). Our results on the single-shell spheroidal model suggest that it is reasonable for the Laplace model to consider the membrane properties in the equatorial region of spheroid-like cells, e.g., erythrocytes when they are oriented with their symmetry axis perpendicular to the field (Gimsa et al., 1996). While the Laplace-ansatz in most cases will have generated effective, model-dependent parameters, the

problem is not as simple for electroorientation since the reorientation, e.g. of ellipsoidal erythrocytes, will not allow the application of a consistent Laplace model suitable for all orientations (see, e.g., Jones, 1995; Miller and Jones, 1993).

We are grateful to Ch. Mrosek for technical assistance. Drs. T. Müller and Th. Schnelle are acknowledged for helpful discussions and for delivering a computer program of the Laplace model. We thank Drs. L. G. Cowell, U. Gimsa, and J. C. Titus-Boudreaux for help with the manuscript.

REFERENCES

Archer, G. P., W. B. Betts, and T. Haigh. 1993. Rapid differentiation of untreated, autoclaved and ozone-treated *Cryptosporidium parvum* oocysts using dielectrophoresis. *Microbios.* 73:165–172.

Arnold, W. M., H. P. Schwan, and U. Zimmermann. 1987. Surface conductance and other properties of latex particles measured by electrorotation. *J. Phys. Chem.* 91:5093–5098.

Asami, K., T. Hanai, and N. Koizumi. 1980. Dielectric approach to suspensions of ellipsoidal particles covered with a shell in particular reference to biological cells. *Jpn. J. Appl. Phys.* 19:359–365.

Asbury, C. L., and G. van den Engh. 1998. Trapping of DNA in nonuniform oscillating electric fields. *Biophys. J.* 74:1024–1030.

Becker, F. F., X.-B. Wang, Y. Huang, R. Pethig, J. Vykoukal, and P. R. C. Gascoyne. 1995. Separation of human breast cancer cells from blood by differential dielectric affinity. *Proc. Natl. Acad. Sci. U.S.A.* 92:860–864.

Eppmann, P., B. Prüger, and J. Gimsa. 1999. Particle characterization by AC-electrokinetic phenomena. 2. Dielectrophoresis of latex particles measured by dielectrophoretic phase analysis light scattering (DPALS). *Colloids Surf., A.* 149:443–449.

Foster, K. R., and H. P. Schwan, 1996. Dielectric properties of tissues. *In* Handbook of Biological Effects of Electromagnetic Fields. C. Polk and E. Postow, editors. CRC Press Inc., Boca Raton, FL. 25–102.

Fuhr, G., J. Gimsa, and R. Glaser. 1985. Interpretation of electrorotation of protoplasts. I. Theoretical considerations. *Stud. Biophys.* 108:149–164.

Fuhr, G., T. Müller, V. Baukloh, and K. Lucas. 1998. High-frequency electric field trapping of individual human spermatozoa. *Hum. Reprod.* 13:136–141.

Fuhr, G., U. Zimmermann, and S. G. Shirley. 1996. Cell motion in time-varying fields: principles and potential. *In* Electromanipulation of Cells. U. Zimmermann and G. A. Neil, editors. CRC Press Inc., Boca Raton, New York, London, Tokyo. 259–328.

Gascoyne, P. R. C., F. F. Becker, and X.-B. Wang. 1995. Numerical analysis of the influence of experimental conditions on the accuracy of dielectric parameters derived from electrorotation measurements. *Bioelectrochem. Bioenerg.* 36:115–125.

Gasperis, G. De, X.-B. Wang, J. Yang, F. F. Becker, and P. R. C. Gascoyne. 1998. Automated electrorotation: dielectric characterization of living cells by real-time motion estimation. *Meas. Sci. Technol.* 9:518–529.

Georgieva, R., B. Neu, V. M. Shilov, E. Knippel, A. Budde, R. Latza, E. Donath, H. Kiesewetter, and H. Bäumler. 1998. Low frequency electrorotation of fixed red blood cells. *Biophys. J.* 74:2114–2120.

Gimsa, J. 1999. New light-scattering and field-trapping methods access the internal structure of submicron particles, like influenza viruses. *In* Electrical Bio-impedance Methods. Applications to Medicine and Biotechnology. P. J. Riu, J. Rosell, R. Bragós, and Ó. Casas, editors. *Ann. NY Acad. Sci.,* New York. 287–298.

Gimsa, J., P. Eppmann, and B. Prüger. 1997. Introducing phase analysis light scattering for dielectric characterization: measurement of traveling-wave pumping. *Biophys. J.* 73:3309–3316.

Gimsa, J., P. Marszalek, U. Löwe, and T. Y. Tsong. 1991. Dielectophoresis and electrorotation of neurospora slime and murine myeloma cells. *Biophys. J.* 60:5–14.

Gimsa, J., T. Müller, and G. Fuhr. 1998. Achieving low driving voltages for micro-motors and fluid pumps by electronic resonance. *In* Microsystem Technologies 98. H. Reichl and E. Obermeier, editors. VDE-Verlag, Berlin, Offenbach. 313–317.

Gimsa, J., T. Müller, Th. Schnelle, and G. Fuhr. 1996. Dielectric spectroscopy of single human erythrocytes at physiological ionic strength: dispersion of the cytoplasm. *Biophys. J.* 71:495–506.

Gimsa, J., and D. Wachner. 1998. A unified RC model for impedance, dielectrophoresis, electrorotation, and induced transmembrane potential. *Biophys. J.* 75:1107–1116.

Grosse, C., and H. P. Schwan. 1992. Cellular membrane potentials induced by alternating fields. *Biophys. J.* 63:1632–1642.

Hagedorn, R., G. Fuhr, T. Müller, and J. Gimsa. 1992. Traveling-wave dielectrophoresis of microparticles. *Electrophoresis.* 13:49–54.

Hölzel, R. 1997. Electrorotation of single yeast cells at frequencies between 100 Hz and 1.6 GHz. *Biophys. J.* 73:1103–1109.

Hölzel, R. 1998. Nystatin-induced changes in yeast monitored by time-resolved automated single cell electrorotation. *Biochim. Biophys. Acta.* 1425:311–318.

Jones, T. B. 1995. Electromechanics of Particles. Cambridge University Press, Cambridge, New York, Melbourne.

Kakutani, T., S. Shibatani, and M. Sugai. 1993. Electrorotation of non-spherical cells: theory for ellipsoidal cells with an arbitrary number of shells. *Bioelectrochem. Bioenerg.* 31:131–145.

Kinosita, Jr., K., and T. Y. Tsong. 1977. Voltage-induced pore formation and hemolysis of human erythrocytes. *Biochim. Biophys. Acta.* 471: 227–242.

Krueger, M., and F. Thom. 1997. Deformability and stability of erythrocytes in high-frequency electric fields down to subzero temperatures. *Biophys. J.* 73:2653–2666.

Landau, L. D., and E. M. Lifschitz. 1985. Elektrodynamik der Kontinua, Vol. 8. Akademie-Verlag, Berlin. (in German).

Maier, H. 1997. Electrorotation of colloidal particles and cells depends on surface charge. *Biophys. J.* 73:1617–1626.

Maxwell, J. C. 1873. Treatise on Electricity and Magnetism. Oxford University Press, London.

Miller, R. D., and T. B. Jones. 1993. Electroorientation of ellipsoidal erythrocytes. *Biophys. J.* 64:1588–1595.

Müller, T., L. Küchler, G. Fuhr, Th. Schnelle, and A. Sokirko. 1993. Dielektrische Einzelzellspektroskopie an Pollen verschiedener Waldbaumarten: Charakterisierung der Pollenvitalität. *Silvia genetica.* 42:311–322.

Pastushenko, V. Ph., P. I. Kuzmin, and Yu. A. Chizmadshev. 1985. Dielectrophoresis and electrorotation: a unified theory of spherically symmetrical cells. *Stud. Biophys.* 110:51–57.

Pastushenko, V. Ph., P. I. Kuzmin, and Yu. A. Chizmadshev. 1988. Dielectrophoresis and electrorotation of cells: unified theory for spherically symmetric cells with arbitrary structure of membrane. *Biol. Mem.* 5:65–78. (in Russian).

Paul, R., and M. Otwinowski. 1991. The theory of the frequency response of ellipsoidal biological cells in rotating electrical fields. *J. Theor. Biol.* 148:495–519.

Pauly, H., and H. P. Schwan. 1959. Über die Impedanz einer Suspension von kugelförmigen Teilchen mit einer Schale. *Z. Naturforsch.* 14b: 125–131. (in German).

Pohl, H. A. 1978. Dielectrophoresis. The behavior of neutral matter in nonuniform electric fields. Cambridge University Press, Cambridge, London, New York, Melbourne.

Prüger, B., P. Eppmann, E. Donath, and J. Gimsa. 1997. Measurement of inherent particle properties by dynamic light scattering: introducing electrorotational light scattering. *Biophys. J.* 72:1414–1424.

Prüger, B., P. Eppmann, and J. Gimsa. 1998. Particle characterization by AC-electrokinetic phenomena. 3. New developments in electrorotational light scattering. *Colloids Surf., A.* 136:199–207.

Sauer, F. A., and R. W. Schlögl. 1985. Torques exerted on cylinders and spheres by external electromagnetic fields. A contribution to the theory of field-induced cell rotation. *In* Interactions Between Electromagnetic Fields and Cells. A. Chiabrera, C. Nicolini, and H. P. Schwan, editors. Plenum Press, New York. 203–251.

Schnelle, Th., H. Glasser, and G. Fuhr. 1997. An opto-electronic technique for automatic detection of electrorotational spectra of single cells. *Cellular Engineering.* 2:33–41.

Schnelle, Th., T. Müller, A. Voigt, K. Reimer, B. Wagner, and G. Fuhr. 1996. Adhesion-inhibited surfaces. Coated and uncoated interdigitated

electrode arrays in the micrometer and submicrometer range. *Langmuir.* 12:801–809.

Sokirko, A. V. 1992. The electrorotation of axisymmetrical cell. *Biol. Membr.* 6:587–600.

Stille, U. 1944. Der Entmagnetisierungsfaktor und Entelektrisierungsfaktor für Rotationsellipsoide. *Archiv f. Elektrotechnik.* 38:91–101. (in German).

Sukhorukov, V. L., H. Mussauer, and U. Zimmermann. 1998. The effect of electrical deformation forces on the electropermeabilization of erythrocyte membranes in low- and high-conductivity media. *J. Membr. Biol.* 163:235–245.

Wang, X.-B., Y. Huang, R. Hölzel, J. P. H. Burt, and R. Pethig. 1993. Theoretical and experimental investigations of the interdependence of the dielectric, dielectrophoretic and electrorotational behaviour of colloidal particles. *J. Phys. D., Appl. Phys.* 26:312–322.

Wang, X., X.-B. Wang, and P. R. C. Gascoyne. 1997. General expressions for dielectrophoretic force and electrorotational torque derived using the Maxwell stress tensor method. *J. Electrostatics.* 39:277–295.

Zimmermann, U., and W. M. Arnold. 1983. The interpretation and use of the rotation of biological cells. *In* Coherent Excitations in Biological Systems. H. Fröhlich and F. Kremer, editors. Springer-Verlag, Berlin. 211–221.